Developmental Biology 335 (2009) 407–417

Contents lists available at ScienceDirect

Developmental Biology

journal homepage: www.elsevier.com/developmentalbiology

# The role of integrin α8β1 in fetal lung morphogenesis and injury

John T. Benjamin [a,f], David C. Gaston [f], Brian A. Halloran [f], Lynn M. Schnapp [g], Roy Zent [b,c,d,e], Lawrence S. Prince [a,b,*]

[a] Department of Pediatrics, Vanderbilt University School of Medicine, Nashville, TN, USA
[b] Department of Cell and Developmental Biology, Vanderbilt University School of Medicine, Nashville, TN, USA
[c] Department of Medicine, Vanderbilt University School of Medicine, Nashville, TN, USA
[d] Department of Cancer Biology, Vanderbilt University School of Medicine, Nashville, TN, USA
[e] Veterans Affairs Hospital, Nashville, TN, USA
[f] Department of Pediatrics, University of Alabama at Birmingham, Birmingham, AL, USA
[g] Department of Medicine, University of Washington, Seattle, WA, USA

ARTICLE INFO

*Article history:*
Received for publication 24 April 2009
Revised 11 September 2009
Accepted 15 September 2009
Available online 19 September 2009

*Keywords:*
Lung development
Branching morphogenesis
Cell–matrix interactions
Cell migration
Fibronectin

ABSTRACT

Prenatal inflammation prevents normal lung morphogenesis and leads to bronchopulmonary dysplasia (BPD), a common complication of preterm birth. We previously demonstrated in a bacterial endotoxin mouse model of BPD that disrupting fibronectin localization in the fetal lung mesenchyme causes arrested saccular airway branching. In this study we show that expression of the fibronectin receptor, integrin α8β1 is decreased in the lung mesenchyme in the same inflammation model suggesting it is required for normal lung development. We verified a role for integrin α8β1 in lung development using integrin α8-null mice, which develop fusion of the medial and caudal lobes as well as abnormalities in airway division. We further show in vivo and in vitro that α8-null fetal lung mesenchymal cells fail to form stable adhesions and have increased migration. Thus we propose that integrin α8β1 plays a critical role in lung morphogenesis by regulating mesenchymal cell adhesion and migration. Furthermore, our data suggest that disruption of the interactions between extracellular matrix and integrin α8β1 may contribute to the pathogenesis of BPD.


## Introduction

The lung develops through multiple generations of airway branching and expansion (Maeda et al., 2007; Metzger et al., 2008; Roth-Kleiner and Post, 2005; Warburton et al., 2000). Epithelial–mesenchymal interactions guide each phase of lung development, with endoderm-derived epithelial tubes invading adjacent mesenchyme. During the initial steps in lung formation, the primitive trachea arises from the ventral surface of the foregut and branches to produce the conducting bronchial airways. In the later canalicular and saccular stages, peripheral airways branch and divide into numerous terminal saccules and alveolar duct networks. Lastly, the most distal airspaces repeatedly divide into smaller alveoli, increasing epithelial surface area available for gas exchange.

Integrin-mediated cell–matrix interactions play a key role in lung development. The bronchi of mice lacking the integrin α3 subunit fail to branch into smaller bronchioles and are lined with undifferentiated cuboidal epithelia (Kreidberg et al., 1996). Mice lacking both integrin subunits α3 and α6 have marked lung hypoplasia, with single right and left lobes (De Arcangelis et al., 1999). Among the integrin ligands, fibronectin is one of the most important during lung development (De Langhe et al., 2005; Roman, 1997). In cultured lung explants, neutralizing antibodies against integrin α5β1 inhibited branching morphogenesis, presumably by blocking integrin-fibronectin interactions in the mesenchymal clefts between adjacent airways (Sakai et al., 2003).

Defective cell–matrix interactions may contribute to abnormal lung development in patients with bronchopulmonary dysplasia (BPD), a complication of preterm birth occurring in over 20% of infants born weighing less than 1500 g (Fanaroff et al., 2007). Arrested saccular stage lung development in BPD leads to dilated saccular airways and reduced alveolar number. The subsequent reduction in lung volumes and surface area available for gas exchange causes hypoxemia and chronic $CO_2$ retention. Clinical data suggest that early exposure to inflammation or infection increases the risk of developing BPD. In experimental models, bacterial endotoxin arrests lung development (Kramer et al., 2008; Moss et al., 2002; Prince et al., 2005), possibly through disrupting normal cell–matrix interactions.

Using a mouse model of BPD, we previously demonstrated that Toll-like receptor agonists and NF-κB activation inhibit saccular airway branching. In fetal mouse lung explants, *Escherichia coli* LPS caused mislocalization of fibronectin from the clefts between developing saccular airways to the lung mesenchyme periphery but

* Corresponding author. Department of Pediatrics, Division of Neonatology Vanderbilt University School of Medicine 9435-A MRB IV 2213 Garland Avenue Nashville, TN 37232-0493, USA.
*E-mail address:* lawrence.s.prince@vanderbilt.edu (L.S. Prince).

0012-1606/$ – see front matter 
doi:10.1016/j.ydbio.2009.09.021

did not change fibronectin biosynthesis or processing (Prince et al., 2005). Based on these observations, in this study we explored what happens to fibronectin receptors in the same model and show decreased expression of integrin α8β1 in the clefts of lung mesenchyme between developing saccular airways. We further show that lung morphogenesis in fetal α8-null mice is abnormal, with defects in lung lobe formation and defective saccular airway branching and division. Thus integrin α8β1 is a critical component of the fetal lung mesenchyme that regulates lung morphogenesis and reduced integrin α8β1 expression may contribute to the abnormal lung development seen in patients with BPD.

## Methods

### *Reagents and animals*

Phalloidin, SYTO13, DAPI, and Alexa-conjugated secondary antibodies were purchased from Invitrogen. Phenol-extracted, gel purified *E. coli* LPS (O55:B5) and Cy3-labeled mouse monoclonal anti α-SMA antibody were from Sigma-Aldrich. Goat anti-α8 integrin antibody was purchased from R&D. Rabbit anti-talin antibody was purchased from Santa Cruz. Rabbit anti-fibronectin was from Abcam. Rabbit anti-α8 was described previously (Schnapp et al., 1995a). The rabbit anti-NG2 and anti-PDGFRβ antibodies were a generous gift from William Stallcup. The anti-Wt-1 antibody was generously supplied by David Bader.

Mice heterozygous for the integrin α8 subunit (Muller et al., 1997) were obtained from the Mutant Mouse Regional Resource Center repository at the University of California at Davis. Animals were genotyped as previously described (Muller et al., 1997). All experimental protocols were approved by the Institutional Animal Care and Use Committees at the University of Alabama at Birmingham and Vanderbilt University.

### *Saccular explant culture*

Our procedure for culturing saccular stage fetal lung explants has been described. (Benjamin et al., 2007; Dieperink et al., 2006; Prince et al., 2005). Briefly, E16 female mice are euthanized and the fetal mouse lungs are isolated and dissected free of surrounding structures. The lung tissue is minced into 0.5–1 $mm^3$ cubes and cultured on an air–liquid interface using permeable supports (Costar Transwell) and serum-free DMEM. Explants were cultured at 37 °C in 95% air/5% $CO_2$ for up to 72 h. LPS was included in culture media at a concentration of 250 ng/ml.

For intact lobe culture, we isolated the accessory and cranial lobes from E15 wild-type and α8-null littermates. The two lobes were placed on permeable supports so that the lobes remained in contact with each other for 48 h in culture. The lobes were then fixed in 4% formaldehyde and stained with both Alexa-594 phalloidin and DAPI.

### *Real-time PCR*

Total RNA was isolated from fetal lung explants and cultured mesenchyme using Trizol reagent and standard protocols (Benjamin et al., 2007). First strand cDNA was synthesized using oligo-dT primers and MMLV reverse transcriptase (Superscript II, Invitrogen). PCR primers designed using Beacon Designer software (BioRad) were validated by performing electrophoresis and melting temperature analysis of the PCR product. Standard concentration curves were done for each primer pair used. Two-step real-time PCR was performed with a BioRad MyiQ thermocycler and SYBR green detection system (BioRad). We normalized gene expression to GAPDH in each sample. The $2^{-\Delta\Delta CT}$ method was used to compare gene expression levels between samples (Arocho et al., 2006). Data between groups were compared by ANOVA to test for significant differences.

### *Histology, immunostaining, microscopy, and image analysis*

Embryonal and newborn lungs were fixed by immersion in 4% paraformaldehyde followed by 70% ethanol. Individual lungs were kept separate throughout processing and later matched to genotype. Fixed lungs were embedded in paraffin and sectioned for staining. For lung morphometry measurements, images of hematoxylin and eosin stained lung sections were obtained using a brightfield microscope. Analysis was performed using the Image Processing Tool Kit (Reindeer Graphics) within Adobe Photoshop and standard measurements (Weibel et al., 1966). For measurement of distal airway volume, at least three separate images from the lungs of 14–16 animals per genotype were analyzed. Three separate litters were used, with each litter containing both wild-type and α8-null animals. Genotype remained unknown during analysis. For mean linear intercept and septal height measurement, 24–32 images were processed for each of 10 different animals per genotype. This allowed measurement of a total of 1300 (α8-null) and 1604 (wild-type) septa. Data were compared by two-way *t*-test.

Elastin-containing elastic fibers were visualized using a Modified Hart's stain including overnight incubation with resorcin–fuchsin and counterstaining with tartrazine in picric acid (Le Cras et al., 2004). For immunostaining, paraffin sections were rehydrated and processed using standard techniques. Antibody staining was detected using Vector Elite ABC kits specific for each primary antibody species. 3,3′-Diaminobenzidine stained sections were briefly counterstained with hematoxylin. Immunofluorescence labeling in explants was performed by fixing tissues in 4% formaldehyde, permeabilizing with 0.1% Triton X-100, blocking in 5% donkey serum, and overnight incubation with primary antibodies. Following secondary antibody addition and DAPI staining, explants were mounted using spacers and imaged using either an inverted Olympus BX-81 microscope with a Hamamatsu Orca ER CCD camera or an Olympus FV1000 laser scanning confocal microscope. Multicolor images were generated using Slidebook. Cultured mesenchymal cells were immunolabeled using standard techniques and imaged using either an inverted fluorescence microscope or a Leica DMIRB laser scanning confocal microscope.

### *Alpha8 cloning and expression*

Full-length cDNA encoding the murine integrin α8 subunit was cloned from E16 BALB/cJ fetal mouse lung RNA. Using an oligodT primer, cDNA was synthesized with MMLV reverse transcriptase. Following RNA degradation, integrin α8 subunit sequence was amplified using gene-specific flanking primers and high fidelity Taq polymerase (Platinum Taq, Invitrogen). The 5′ primer contained the inserted Kozak sequence GCCACC prior to the start ATG codon. The PCR product was digested with BamHI and EcoRV and subcloned into the pCDF expression vector (System Biosciences), which expresses copGFP from a separate downstream expression cassette. After sequence verification, cDNA was transfected into primary fetal lung mesenchymal cells using Lipofectamine Plus reagent. GFP expression in transfected cells was visible between 24 and 48 h following transfection.

### *Live-cell and time lapse microscopy*

A live-cell imaging system based on a Zeiss Axiovert microscope was used for time-lapse imaging of cells and explants. Temperature, humidity, and 5% $CO_2$ atmosphere were all accurately maintained in an enclosed stage incubator. An automated *xy* stage allowed imaging of multiple fields, and phototoxicity was prevented using a automated shutter. Images were acquired using an EM-CCD camera (DV885) and iQ software (both from Andor). Multi-TIFF file movies were converted to .avi and Quick-Time format using iQ and iMovie (Apple), respectively. For cell tracking experiments, time-lapse move files of

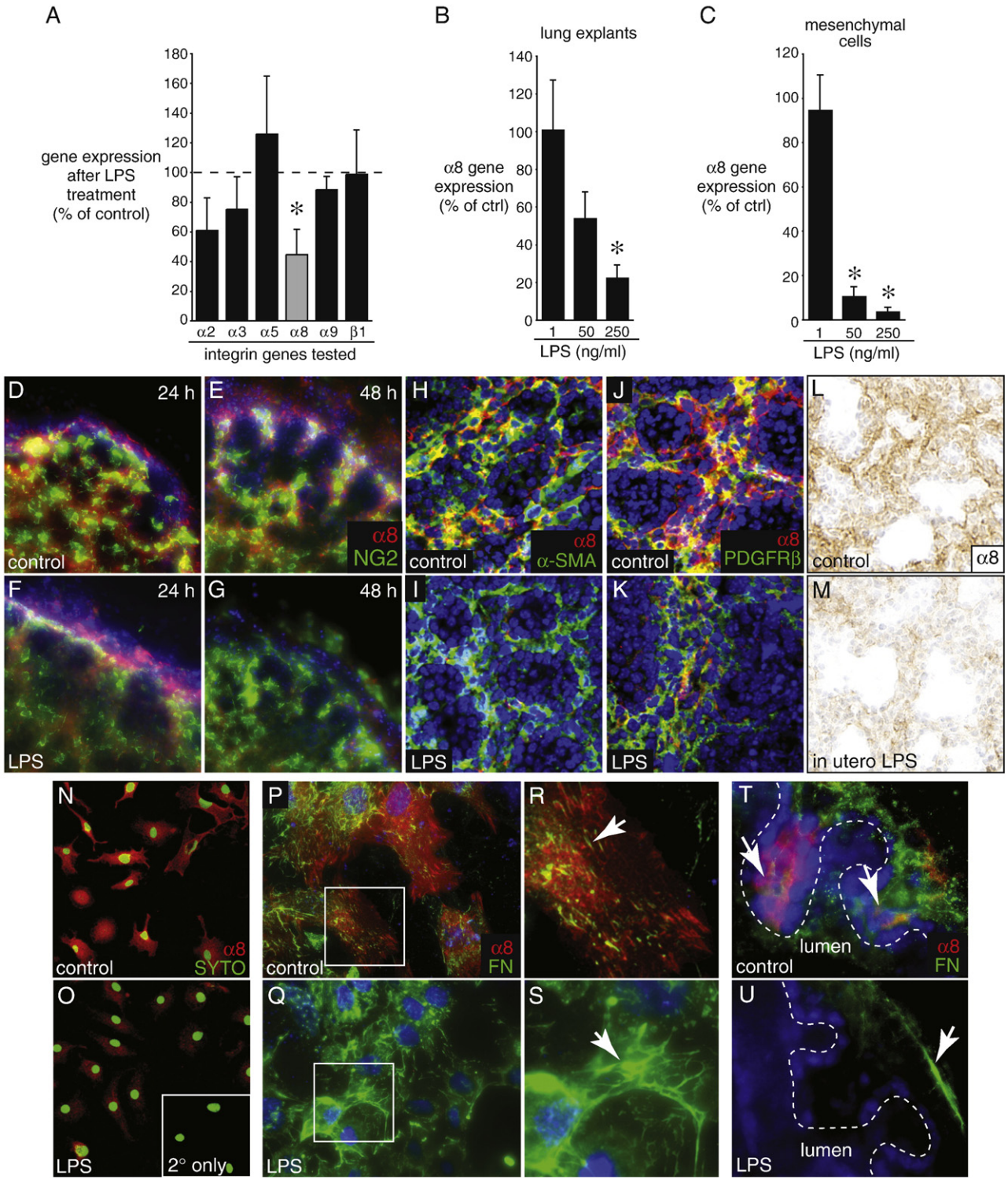


**Fig. 1.** LPS inhibits integrin α8β1 expression in fetal mouse lung. (A) *E. coli* LPS (250 ng/ml for 72 h) inhibited integrin α8 subunit expression in E16 saccular stage mouse lung explants. Integrin expression was measured by real-time PCR, and fold change was calculated using the $2^{-\Delta\Delta CT}$ method. For each gene, data are represented as the percentage of control values obtained from untreated samples (*$P<0.05$, $n=5$–9; each sample measured in triplicate). (B) Effect of LPS on integrin α8 subunit expression was concentration dependent. E16 explants were treated with 1, 50, or 250 ng/ml LPS for 72 h. Gene expression measured by Real-Time PCR (*$P<0.05$, $n=4$). (C) LPS inhibited integrin α8 subunit expression in primary fetal lung mesenchymal cells in a concentration dependent manner (*$P<0.05$, $n=3$). (D–K) LPS reduced integrin α8 subunit expression by immunomicroscopy. Control (D, E, H, J) and LPS-treated (F, G, I, K) explants were cultured for 24 h (D, F) and 48 h (E, G–K), fixed, and labeled with antibodies against integrin α8 and the mesenchymal cell markers NG2 (D–G), α-SMA (H, I), or PDGFRβ (J, K). Nuclei were labeled with DAPI (blue). (L, M) LPS inhibits integrin α8 expression in vivo. Mice were injected with sterile, endotoxin-free saline (control) or LPS on E15. Lungs were isolated on E17 (48 h following injection), fixed, sectioned, and immunostained for integrin α8. (N–S) LPS inhibited integrin α8 subunit expression in cultured fetal lung mesenchymal cells. (N, O) Immunostaining of control and LPS-treated fetal mouse lung mesenchymal cells for integrin α8 subunit expression (red) shows widespread decrease in α8β1 expression. Nuclei stained with SYTO13 (green). Inset in (O) shows background fluorescence when primary antibody omitted. (P–S) Integrin α8β1 colocalizes with fibronectin in fetal lung mesenchymal cells. Control (P, R) and LPS-treated (Q, S) mesenchymal cells were immunostained with antibodies against fibronectin (green) and integrin α8 (red). Higher magnification of areas indicated in (P, Q) are shown in (R, S). Arrows indicate fibronectin staining. (T, U) Integrin α8β1 and fibronectin colocalization in the clefts between branching airways. Control (T) and LPS-treated (U) fetal lung explants were immunolabeled with antibodies against the integrin α8 subunit (red) and fibronectin (green). Arrows indicate fibronectin staining.

GFP-labeled cells within explants were analyzed using the Particle Tracking Protocol within Slidebook (Intelligent Imaging Innovations). Labeled cells were identified by size and fluorescence intensity. Cells were excluded if they were not detected in the focal plane for at least three continuous time points. Data on cell position, velocity, and displacement were exported to Excel for analysis. Kymographs were generated by projecting the image intensity along a single line crossing a cell on the *y*-axis and changes in image intensity over time on the *x*-axis. For time lapse imaging of airway branching in lung explants, E16 explants were allowed to recover for 12 h after isolation. Individual explants were then imaged by brightfield microscopy using a 5× objective, capturing images every 15 min for 36 h.

### *Cell migration*

Modified Boyden chambers were prepared from 10-mm tissue culture inserts (Nunc) with 8 μm pore size polycarbonate membranes. The membranes were first permeated with 10 μg/ml fibronectin or 10 μg/ml type I collagen (Calbiochem) for 1 h at 37 °C. The filters were then washed, and 25,000 cells were added to the apical side of each filter. DMEM with 10% fetal calf serum was included in both sides of the chamber. Following 16 h of culture, cells that had migrated through the filter to the basal side were stained with DAPI, visualized by fluorescence microscopy, and counted. Wild-type and α8-null cells were always tested in parallel.

## Results

### *LPS inhibits integrin α8β1 expression*

We previously showed that LPS-induced inflammation disrupts the normal distribution of fibronectin in the fetal lung mesenchyme, leading to an arrest in saccular airway branching (Benjamin et al., 2007; Prince et al., 2005). As integrins α5β1, α8β1, and α9β1 are expressed in the fetal lung and can bind fibronectin (Coraux et al., 1998; Schnapp et al., 1995b; Wang et al., 1995; Wu and Santoro, 1996), we used real-time PCR to investigate the expression of these integrins in fetal mouse lung explants exposed to LPS. Of the integrins we tested, only α8β1 expression was inhibited in a concentration dependent manner. There were no significant changes in expression of the collagen receptor α2β1 or the laminin receptor α3β1 (Figs. 1A, B). LPS also inhibited expression of the α8 subunit in a concentration-dependent manner in primary fetal mouse lung mesenchymal cells (Fig. 1C). Immunostaining of cultured lung explants confirmed

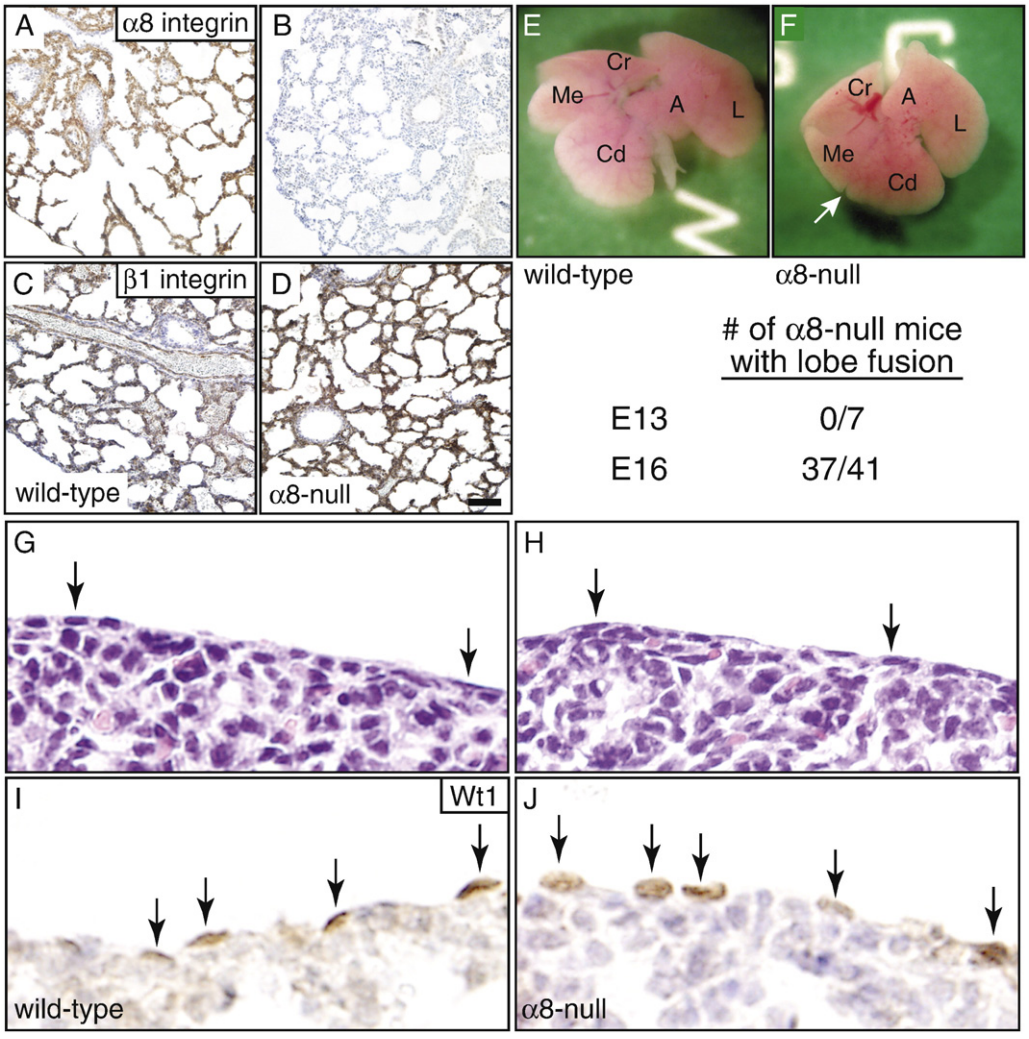


**Fig. 2.** Abnormal lung lobe formation in integrin α8-null mice. (A–D) Immunostaining of newborn wild-type (A, C) and α8-null (B, D) lungs using antibodies against integrin α8 (A, B) or integrin β1 (C, D). Scale bar, 100 μm. (E, F) α8-Null lungs display fusion of right medial and caudal lobes at E16. (E) Wild-type lungs with distinctly separate left lung (L), cranial (Cr), medial (Me), caudal (Cd), and accessory (A) lobes comprising the right lung. (F) Lungs from α8-null fetus showing fusion of the right medial (Me) and caudal (Cd) lobes. Arrow indicates fissure where intralobar division would normally be present. (G, H) Hematoxylin and eosin (H and E) stain of wild-type (G) and α8-null (H) lungs demonstrate presence of flattened, elongated mesothelial cells along the lung periphery (arrows). (I, J) Immunostaining for the mesothelial marker Wt-1 confirms the presence of mesothelial cells (arrows) in both wild-type (I) and α8-null (J) lungs.

expression of the α8 subunit in the mesenchyme between saccular airways (Figs. 1D–K). Expression levels decreased between 24 and 48 h following LPS treatment (Figs. 1D–G). While LPS reduced α8 subunit expression, we did not observe changes in the mesenchymal cell markers NG2, α-SMA, or PDGFRβ (Figs. 1D-K). We also measured reduced α8 subunit expression in the lungs of mice exposed in utero to LPS (Figs. 1L, M). LPS inhibited α8 staining in cultured mesenchymal cells and this decrease correlated with changes in the fibronectin staining pattern in the majority of cells examined (Figs. 1N–S). Integrin α8β1 and fibronectin colocalized to the mesenchyme between newly formed saccular airways (arrows in Fig. 1T) and like α8, fibronectin expression was diminished in the mesenchymal clefts between saccular airways in LPS-treated explants (Fig. 1U). Therefore, integrin α8β1 appeared to be a specific target of LPS in the fetal lung mesenchyme.

*Abnormal lung development in integrin α8-null mice*

As LPS decreased integrin α8β1 expression in the mesenchyme of fetal lungs in addition to disrupting normal lung development, we investigated the role of this integrin in normal lung development by studying the α8-null mouse. The majority of newborn α8-null mice have renal dysgenesis and die soon after birth (Haas et al., 2003; Muller et al., 1997); however, when embryos were examined at E18 and postnatal day 0, mice were found in the expected percentages of 24% wild-type, 48% heterozygotes, and 28% homozygotes. There were no differences in gross appearance, crown-rump length, or the amount of amniotic fluid between fetal and newborn wild-type and α8-null pups (not shown).

We verified that the integrin α8 subunit was deleted in the α8-null mice by immunohistochemistry. (Figs. 2A, B). As expected, expression of the $\beta_1$-integrin subunit was similar in wild-type and α8-null lungs (Figs. 2C, D). When lung formation was examined at E13, all five lobes (four right, one left) appeared to form normally regardless of genotype. However, by E16 the lungs from α8-null animals were grossly abnormal, with fusion of the medial and caudal lobes of the right lung occurring in 37 of 41 E16 homozygotes (90%), but never in wild-type or heterozygotes (Figs. 2E, F). This lobe fusion was not due to the lack of mesothelium formation, as both wild-type and α8-null lungs were lined with flat, Wt-1-positive mesothelial cells (Figs. 2G–J).

On histological examination, the airspaces of α8-null lungs at E18 and later also appeared abnormal, with more dilated saccular airways that were irregular in size and shape. The dilated saccular airways in

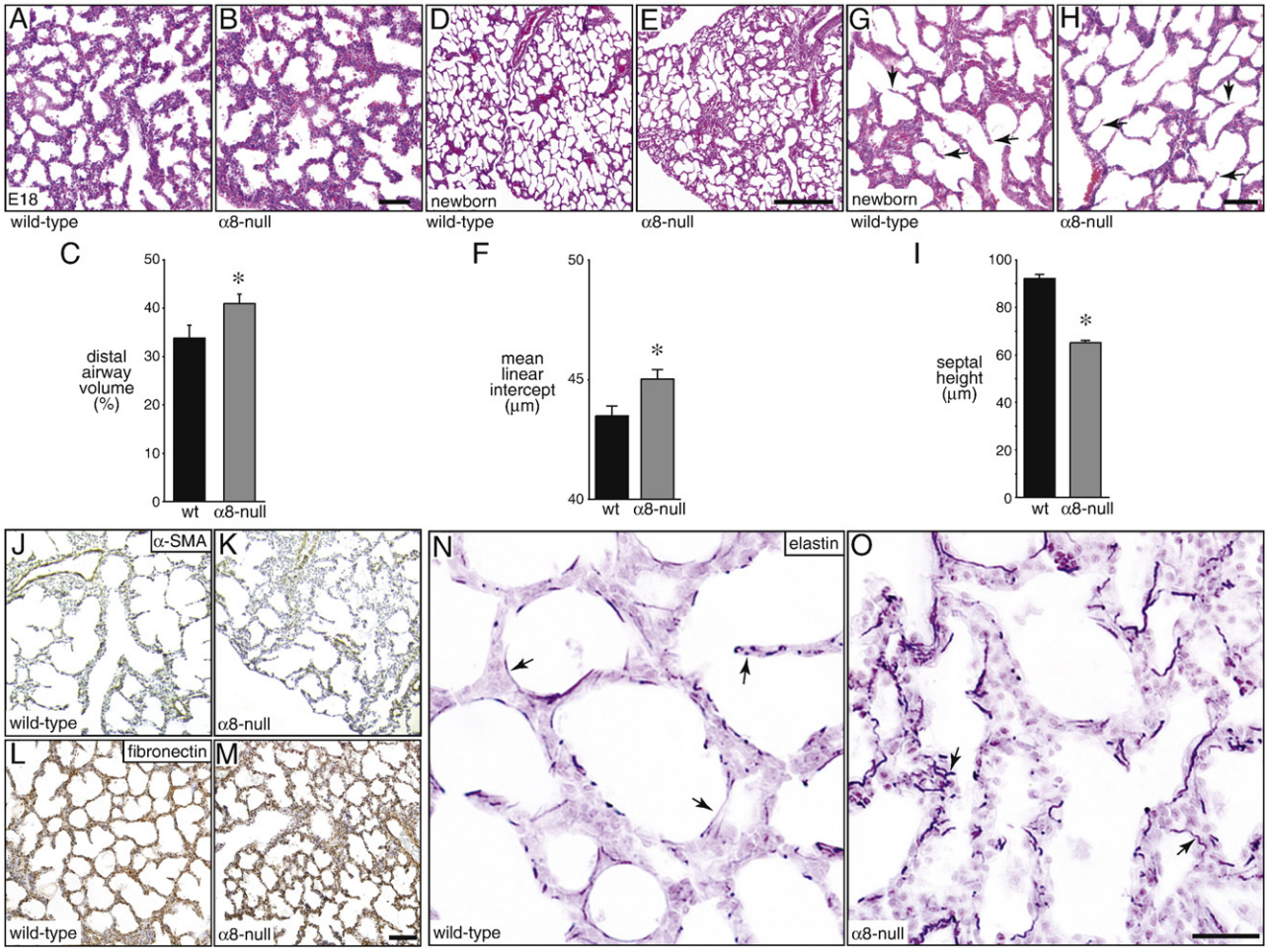


**Fig. 3.** Abnormal airway morphogenesis in integrin α8-null mice. (A–C) Dilated airways in E18 α8-null lungs. Lungs from E18 wild-type (A) and α8-null (B) littermates were fixed, sectioned, and stained with H and E. Scale bar 100 μm. (C) Distal airway volume was increased in α8-null lungs compared to wild-type littermates when measured by morphometry (*$P<0.05$). (D–I) Reduced airway division and septal height in newborn α8-null mice. Lungs from wild-type and α8-null littermates were fixed, sectioned, and stained with H and E. (D, E) Low-power images show more cystic appearance of α8-null lungs with heterogeneous airway size. Scale bar 500 μm. (F) Increased airway diameter in α8-null mice as measured by mean linear intercept (*$P<0.01$, $n=32$). (G, H) Higher magnification images show reduced septal height in α8-null lungs. Arrows indicate representative septa. Scale bar 100 μm. (I) Newborn lungs from α8-null mice had shorter septa between airways compared to wild-type littermates (*$P<0.001$; $n=24$–32, >1300 septa measured). (J–M) Immunostaining of newborn wild-type (J, L) and α8-null (K, M) lungs using an antibody against α-smooth muscle actin (α-SMA; J, K) or fibronectin (L, M). Scale bar, 100 μm. (N, O) Abnormal elastic fibers in α8-null newborn mouse lungs. Newborn lungs from wild-type (N) and α8-null littermates (O) were fixed, sectioned, and stained with a modified Hart's stain to visualize elastic fibers. Arrows indicate elastic fibers, which appear more wavy and irregular in α8-null lungs. Scale bar, 100 μm.

α8-null mice resulted in an increased luminal airway volume compared to wild-type littermates (Figs. 3A–C). We did not observe defects in bronchial airway formation in α8-null animals at earlier stages of development (not shown). Newborn α8-null lungs also displayed defective lung morphogenesis with irregular, dilated airspaces adjacent to areas with small or collapsed airways (Figs. 3D, E). The mean linear intercept, which represents airspace size, was increased in α8-null lungs (Fig. 3F). In addition, septa dividing newly formed airspaces were shorter in α8-null newborn lungs (Figs. 2G–I). We stained newborn lung sections for components of alveolar septa to better characterize this defect. α-Smooth muscle actin, a marker for myofibroblasts and peribronchial smooth muscle, appeared similar in wild-type and α8-null lungs (Figs. 3J, K). The fibronectin immunostaining pattern was likewise similar in wild-type and α8-null newborn lungs (Figs. 3L, M). However, elastin staining showed abnormally wavy and short elastic fibers in α8-null lungs compared to controls (arrows, Figs. 3N, O). The total amount of elastin did not appear different between wild-type and α8-null lungs. These results demonstrate that expression of the mesenchymal integrin α8β1 in the fetal lung is required for normal saccular airway morphogenesis.

We further tested the role of integrin α8β1 in saccular airway morphogenesis using E16 saccular stage fetal lung explants, which allows direct visualization of airway formation independent of extrapulmonary influences (Benjamin et al., 2007; Dieperink et al., 2006; Prince et al., 2005; Prince et al., 2004). Absent integrin α8 subunit expression in α8-null mice was confirmed by immunostaining (Figs. 4A, E). After 72 h of culture, α8-null explants displayed heterogeneous defects in saccular airway formation. α8-Null explants had more dilated saccular airways with fewer divisions and less elongation (Figs. 4F–H). To understand how these abnormal saccular airways formed, we performed time-lapse imaging of wild-type and α8-null explants. Both wild-type and α8-null explants appeared similar at the beginning of the experiment, but some airways in α8-null explants became very dilated, failing to divide and elongate into new airway generations (Figs. 4I, J). Therefore absence of integrin α8β1 in the fetal lung mesenchyme leads to increased saccular airway dilation and defective airway division.

As saccular airway size and shape may be regulated by dynamic interactions between mesenchyme and the subepithelial extracellular matrix, we visualized the behavior of mesenchymal cells adjacent to developing saccular airways. To randomly label mesenchymal cells in wild-type and α8-null saccular stage explants with GFP, we initially cultured explants for 24 h following isolation. This recovery period allowed recovery and enclosure of the epithelial cells lining saccular airways. Because epithelial cells were then covered by mesenchyme and not in direct contact with culture media, we could add a low titer

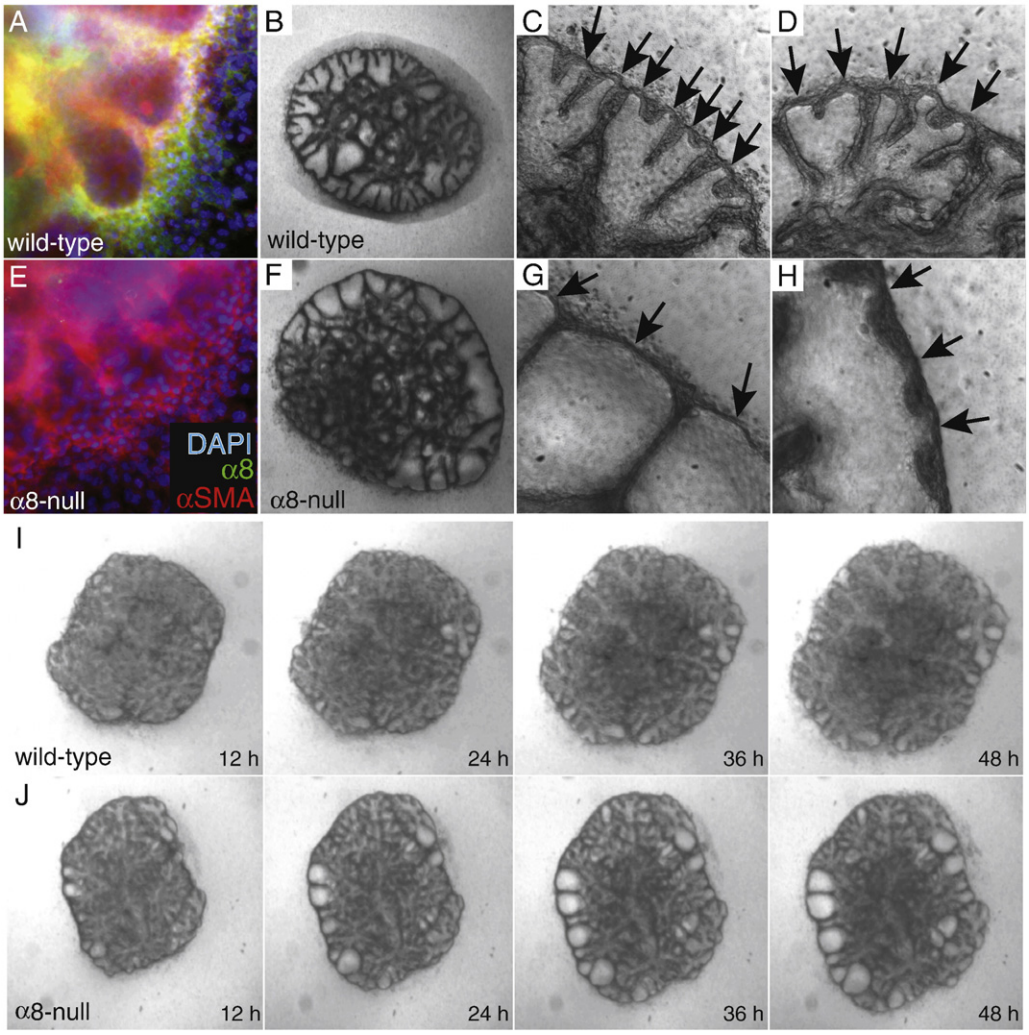


**Fig. 4.** Increased saccular airway dilation in α8-null fetal lung explants. (A, E) Immunofluorescent images of E16 explants show expression of the integrin α8 subunit (green) and α-SMA (red) in wild-type mesenchyme (A) but only α-SMA in α8-null explants (E). (B–D) Saccular airways along the periphery of wild-type explants branch, elongate and divide in culture. Arrows indicate newly forming explants. (F–H) Airways in α8-null explants become dilated, with either no new branches (G) or small, rudimentary airway branches (H). (I, J) Time-lapse still photomicrographs of wild-type and α8-null explants show progressive dilation of airways along the periphery of α8-null explants. Time-lapse movies of this experiment are included in Supplemental Data.

of GFP-expressing adenovirus to label a random subset of mesenchymal cells along the explant periphery. Confocal images obtained 24 h following Ad-GFP infection confirmed that GFP expressing cells co-localized with antibodies against the mesenchymal marker vimentin but did not colocalize with the epithelial marker E-cadherin (Figs. 5A, B).

We then performed time-lapse fluorescence microscopy to monitor the movement of GFP-expressing cells in wild-type and α8-null explants. Mesenchymal cells within wild-type explants formed stable processes around newly formed saccular airways (Fig. 5C), however this was not the case in the α8-null explants, where cells appeared to randomly migrate throughout the mesenchyme (Fig. 5D). Cell-tracking measurements of GFP-expressing cells demonstrated that α8-null cells migrated more quickly and randomly within the developing explants (Figs. 5E, F). These data suggest that loss of integrin α8β1 alters mesenchymal cell behavior during lung development.

*Integrin α8 subunit expression promotes focal contacts and stress fiber formation*

One possible explanation for the phenotype of the lungs in α8-null mice is that mesenchymal cells lacking integrin α8β1 may be unable to form normal cell–matrix interactions and maintain tension around developing saccular airways. We therefore tested if cultured α8-null fetal lung mesenchymal cells isolated from E16 mice could form focal contacts and stress fibers when adhering to fibronectin. Wild-type cells formed multiple talin-positive focal contacts, which aligned with actin stress fibers that extended across the cells (Figs. 6A–C); however, the α8-null cells developed fewer focal contacts which were aligned to short actin filaments that did not traverse the cell body. The majority of actin staining in α8-null cells was perinuclear compared to the transcellular stress fibers seen in wild-type cells (Figs. 6D–F). To verify that these changes in stress fiber formation were due to the loss of integrin α8β1, we transfected primary fetal

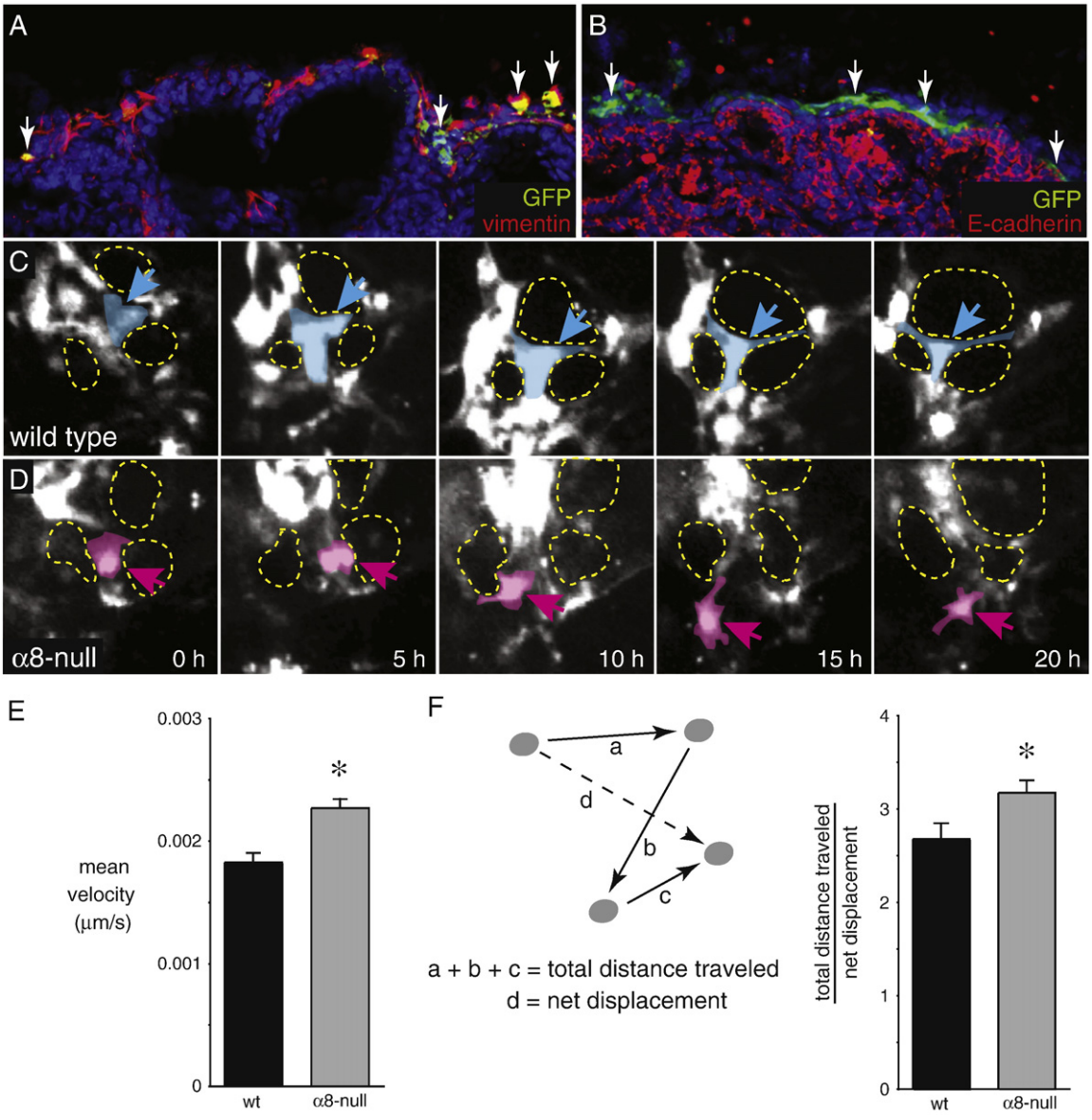


**Fig. 5.** Increased mesenchymal cell migration in α8-null fetal lung explant tissue. E16 explants from wild-type and α8-null littermates were infected with GFP expressing adenovirus (Ad-GFP) to randomly label mesenchymal cells. (A, B) Confocal imaging of Ad-GFP infected explants showing GFP colocalization with the mesenchymal marker vimentin (A) but no overlap with the epithelial marker E-cadherin (B). (C, D) Time-lapse fluorescence microscopy followed cells in wild-type (C) and α8-null (D) explants for 20 h. Arrows track individual wild-type (blue) and α8-null (pink) cells over time; yellow dashed lines mark developing airways. Movies included in Supplemental Data. (E) Mean velocity of GFP-expressing cells in wild-type and α8-null explants as measured by cell tracking (* $P < 0.05$, 423–852 cells within four different explants were tracked). (*F*) Randomness of cell migration measured by dividing the total distance traveled by each cell by the net displacement (distance between beginning and final position; * $P < 0.05$).

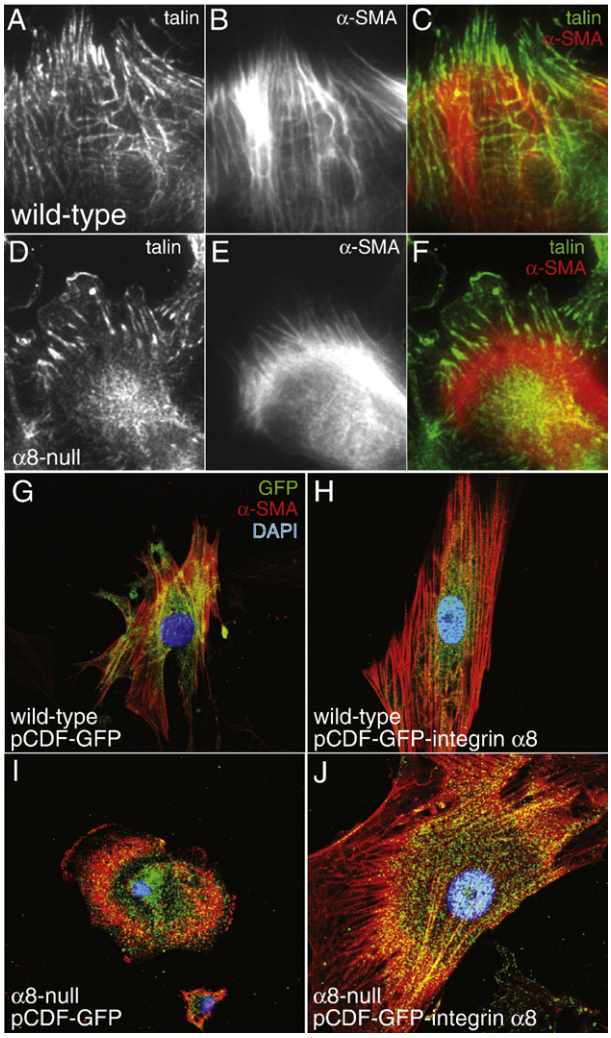


**Fig. 6.** Integrin α8 subunit expression is required for normal focal adhesion and stress fiber formation in fetal lung mesenchymal cells. Wild-type (A–C) and α8-null (D–F) fetal lung mesenchymal cells were cultured on fibronectin-coated slides and immunolabeled with antibodies against talin (A, D; green in C, F) and α-SMA (B, E; red in C, F). (G–J) Transfection of fetal lung mesenchymal cells with integrin α8 increases actin stress fiber formation. Wild-type (G, H) and α8-null (I, J) fetal lung mesenchymal cells plated onto fibronectin were transfected with either pCDF-GFP control vector (G, I) or pCDF-GFP-integrin α8 (H, J). Cells were fixed and immunostained with an antibody against α-SMA. Transfected cells were identified by GFP expression, driven by a separate expression cassette in the pCDF vector. Nuclei were labeled with DAPI.

lung mesenchymal cells from α8-null and wild-type lungs with integrin α8 subunit cDNA cloned into a bicistronic vector that expresses both integrin α8 and GFP. While α8-null cells expressing GFP alone again appeared rounded with perinuclear actin (Fig. 6I), cells transfected with the integrin α8 subunit developed organized stress fibers (Fig. 6J). These data suggested that integrin α8β1 promotes formation of focal contacts and transcellular stress fibers in fetal lung mesenchymal cells plated on fibronectin.

To further test if loss of integrin α8β1 leads to increased mesenchymal cell migration, we measured random migration of fetal lung mesenchymal cells by performing both live-cell microscopy and haptotactic migration assays in Boyden chambers. As seen in Fig. 7, wild-type cells adhered strongly to fibronectin, with stable cell processes and few areas of membrane ruffling (Fig. 7A); however, α8-null cells had large areas of membrane ruffling and turnover, leading to increased cell movement (Fig. 7B). Kymographs show the relative stability of wild-type cells on fibronectin compared to the dramatic membrane dynamics in α8-null cells (Fig. 7C; full time-lapse movies of wild-type and α8-null cells are included in Supplemental Data). Boyden chamber experiments confirmed these differences in migration, with more α8-null cells migrating through fibronectin-coated pores than wild-type cells (Fig. 7D). Migration through collagen-coated pores was not significantly different between wild-type and α8-null cells. Thus, consistent with our data in cultured explants, loss of integrin α8β1 leads to abnormal cell migration.

How might loss of integrin α8β1 lead to lobe fusion? One possibility is that the inherent properties of increased migration of α8-null mesenchymal cells lead to fusion of adjacent lung lobes. To investigate this, we cultured the cranial and accessory lobes from E15 wild-type and α8-null littermates, which are not positioned in close proximity *in vivo*, on nylon filters for 48 h (Figs. 7E–H). Following this culture period, the wild-type lobes remained separate with no signs of attachment and floated free of each other during fixation and phalloidin staining (Figs. 7E, F). In contrast, the α8-null lobes grew together, forming multiple cellular bridges between adjacent lobes that remained intact during processing (Figs. 7G, H). These data suggest that the defects in cell–matrix interactions and cell migration of α8-null mesenchymal cells promote lung lobe fusion.

## Discussion

In preterm infants with BPD, inflammation contributes to arrested fetal lung development by disrupting the epithelial-mesenchymal interactions required for normal airway branching (Benjamin et al., 2007; Kramer et al., 2008; Prince et al., 2005). In this study we show that *E. coli* LPS, which prevents saccular airway branching, inhibits expression of the fibronectin receptor integrin α8β1 in lung mesenchymal cells. We further demonstrate that α8-null mice have fusion of their medial and caudal lobes, dilation of saccular airways, shortened alveolar septa, and disorganized elastic fibers. As many of these features overlap with those found in BPD (Coalson, 2003), we speculate that reduced expression of integrin α8β1 following exposure to inflammation may play a role in BPD pathogenesis.

The wavy, irregular elastic fibers in α8-null lungs suggest that integrin α8β1 is required for establishing and maintaining mechanical tension around saccular airways and developing alveoli. Similar cellular defects were observed in α8-null kidneys, where mechanical stability of the renal glomerular capillaries is abnormal in α8-null mice that survive to adulthood (Hartner et al., 2002). Induction of hypertension in these mice leads to increased mesangial expansion and glomerular destruction. These findings are consistent with our results implicating integrin α8 in regulating mechanical tension around developing saccular airways. In addition, the defects in α8-null airway division imply that integrin α8β1 facilitates the division of expanding airways into new branches. Our data do not completely exclude other processes that could affect saccular airway development, including changes in fluid transport and cell signaling. However, the mesenchymal expression of α8β1 and its role in binding extracellular matrix and mesenchymal cell membrane dynamics support the role of integrin α8β1 in regulating morphogenesis through cell–matrix interactions. α8-Null mesenchymal cells formed fewer focal contacts without transcellular actin stress fibers and were more mobile, with increased membrane ruffling and turnover both in vivo and in vitro. These observations suggest that integrin α8β1 regulates mesenchymal cell membrane dynamics during fetal lung morphogenesis.

Fusion of α8-null lung lobes both in vivo and in vitro is a consequence of mesenchymal and mesothelial cell abnormalities. α8-Null lungs do have a mesothelial layer (Fig. 2), but loss of integrin α8β1 may cause abnormal mesothelial cell function, potentially leading to both defective saccular airway branching and lung lobe fusion. Only the cranial and medial lobes fused in vivo, likely due to the intimate approximation of these two lobes during development. Defects in lobe formation have been reported for mice with defects in

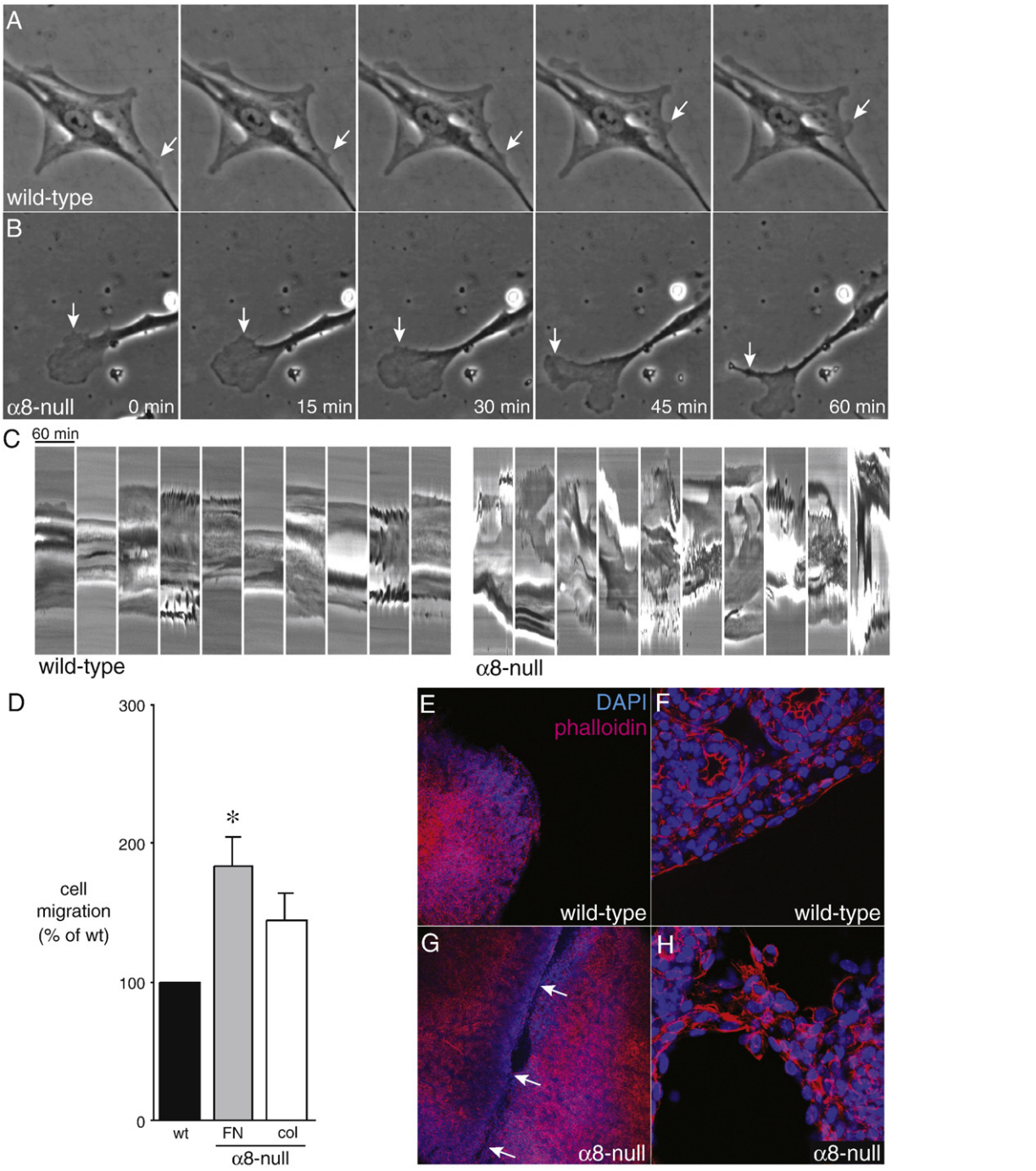


**Fig. 7.** Increased migration of α8-null fetal lung mesenchymal cells leading to lung lobe fusion. (A, B) Wild-type and α8-null fetal lung mesenchymal cells were plated onto fibronectin and imaged by time-lapse phase contrast microscopy. Images were taken each minute for 1 h. Arrows indicate areas of membrane ruffling. Movies from three different cells are included as Supplemental Data. (C) Kymographs of wild-type and α8-null mesenchymal cells. Lines were drawn across individual cells and the phase-contrast intensities were plotted over 60 min. Upward and downward deflections indicate movement of the cell membranes. Kymographs from 10 different cells are shown for each genotype. (D) Increased haptotactic migration by α8-null mesenchymal cells. Wild-type and α8-null cells were placed in fibronectin-coated or collagen-coated Boyden chambers. For each replicate, the number of α8-null cells migrating through the filter was normalized to wild-type (*$P < 0.05$, $n = 8$). (E–H) Fusion of α8-null lung lobes in vitro. The cranial and accessory lobes from wild-type (E, F) and α8-null (G, H) E16 mice were cultured for 48 h, fixed, and stained with Alexa547-conjugated phalloidin and DAPI. Low magnification fluorescence images are shown in (E, G). Higher magnification images (F, H) revealed intact cell layers surrounding the wild-type lobes but cellular bridges and fusion between the α8-null lobes.

Gli2 (Motoyama et al., 1998), Gata4 (Ackerman et al., 2007), foxf1 (Lim et al., 2002), fog2 (Ackerman et al., 2005), laminin $\alpha_5$ (Nguyen et al., 2002), the integrin subunits α3 and α6 (De Arcangelis et al., 1999) and in Hip overexpressing animals (an inhibitor of Shh signaling; Chuang et al., 2003). Unlike α8-null animals, these mutant mice have either global defects in lung formation (Hip, Gli2, foxf1), complete agenesis of single lobes (Gata4, fog2) or disrupted pleural basement membrane formation (laminin α5, integrin α3/α6). Thus α8-null mice display a novel defect in lung development where distinct lobes fuse together after they have formed.

Defects in kidney function that reduce normal amniotic fluid production could potentially cause secondary affects on lung growth as part of the Potter sequence (Nakamura et al., 1985; Perlman et al., 1976). While integrin α8β1 is required for normal renal development,

we did not observe reduced amniotic fluid or gross abnormalities in α8-null mice. In addition, saccular airway development was abnormal in α8-null lung explants cultured ex vivo, removed from potential effects of amniotic fluid production. We believe the data therefore point to primary abnormalities in α8-null lungs.

Integrin α8β1 can bind multiple ligands, and this study does not determine if interactions between α8β1 and a specific, individual matrix protein ligand mediate normal lung development. In the developing kidney, interactions between integrin α8β1 and nephronectin regulate GDNF signaling (Linton et al., 2007). We have not yet determined if a similar process occurs in the developing mouse lung. While both fibronectin and tenascin-C bind integrin α8β1 and play a role in lung development, fibronectin's role in branching morphogenesis is better described (Prince et al., 2005; Sakai et al., 2003; Young et al., 1994). Fibronectin localizes to the clefts between epithelial tubes in the branching lung, submandibular gland, and kidney. During cleft formation, fibronectin interferes with intercellular E-cadherin, producing instability of epithelial monolayers and allowing invagination of epithelial-lined structures (Sakai et al., 2003). In lung explants treated with LPS, displacement of fibronectin from these clefts may prevent normal airway branching and division (Prince et al., 2005). We speculate that decreased integrin α8β1 expression leads to abnormal fibronectin localization in mouse lungs following LPS exposure, and may contribute to the arrested lung development in BPD.

Inflammation-mediated arrest in lung development may be an early step in BPD pathogenesis. While the association between inflammation and BPD is clear (Speer, 2003; Willet et al., 2001; Young et al., 2005), the molecular mechanisms explaining how lung development is arrested have not been identified. Inflammation may disrupt lung formation by altering growth factor expression and epithelial differentiation (Benjamin et al., 2007; Kramer et al., 2008; Prince et al., 2004), each potentially contributing to BPD. In addition, multiple studies have implicated abnormal matrix synthesis, turnover, or localization in BPD pathogenesis (Alejandre-Alcazar et al., 2007; Bland et al., 2007; Sinkin et al., 1998; Thibeault et al., 2003). The data presented here show that integrin α8β1 is critical for normal lung development and is inhibited by inflammation. Features of the α8-null lung phenotype, including dilated saccular airways and shortened alveolar septa, overlap with BPD pathology. Our findings establish a new molecular mechanism that explains how integrin–matrix interactions regulate lung morphogenesis and suggest that defects in these interactions could contribute to diseases of abnormal lung development.

## Acknowledgments

The investigators would especially thank Jin-Hua Liu, Lorene Batts, and Sara Darbar for technical assistance, Anne Woods and Timothy LeCras for their helpful suggestions, and our colleagues for critical review of the data and manuscript. This work was supported by grant support from iNO Therapeutics (J.T.B.), the American Lung Association (L.S.P.), March of Dimes (L.S.P), NHLBI (R01 HL086324, L.S.P), NIDDK (RO1 DK069921, R01 DK075594, P01 DK65123, R.Z), Veterans Affairs (Merit Award R.Z.) and American Heart Association (Established Investigator Award R.Z). Confocal imaging was performed in part through the use of the VUMC Cell Imaging Shared Resource (supported by NIH grants CA68485, DK20593, DK58404, HD15052, DK59637 and EY08126). Dr. Benjamin's current address is in the Department of Pediatrics, University of South Alabama, Mobile, AL.

## Appendix A. Supplementary data

Supplementary data associated with this article can be found, in the online version, at doi:10.1016/j.ydbio.2009.09.021.

## References

Ackerman, K.G., Herron, B.J., Vargas, S.O., Huang, H., Tevosian, S.G., Kochilas, L., Rao, C., Pober, B.R., Babiuk, R.P., Epstein, J.A., Greer, J.J., Beier, D.R., 2005. Fog2 is required for normal diaphragm and lung development in mice and humans. PLoS Genet. 1, 58–65.

Ackerman, K.G., Wang, J., Luo, L., Fujiwara, Y., Orkin, S.H., Beier, D.R., 2007. Gata4 is necessary for normal pulmonary lobar development. Am. J. Respir. Cell. Mol. Biol. 36, 391–397.

Alejandre-Alcazar, M.A., Kwapiszewska, G., Reiss, I., Amarie, O.V., Marsh, L.M., Sevilla-Perez, J., Wygrecka, M., Eul, B., Kobrich, S., Hesse, M., Schermuly, R.T., Seeger, W., Eickelberg, O., Morty, R.E., 2007. Hyperoxia modulates TGF-beta/BMP signaling in a mouse model of bronchopulmonary dysplasia. Am. J. Physiol. Lung Cell. Mol. Physiol. 292, L537–549.

Arocho, A., Chen, B., Ladanyi, M., Pan, Q., 2006. Validation of the 2-DeltaDeltaCt calculation as an alternate method of data analysis for quantitative PCR of BCR-ABL P210 transcripts. Diagn. Mol. Pathol. 15, 56–61.

Benjamin, J.T., Smith, R.J., Halloran, B.A., Day, T.J., Kelly, D.R., Prince, L.S., 2007. FGF-10 is decreased in bronchopulmonary dysplasia and suppressed by Toll-like receptor activation. Am. J. Physiol. Lung Cell. Mol. Physiol. 292, L550–L558.

Bland, R.D., Xu, L., Ertsey, R., Rabinovitch, M., Albertine, K.H., Wynn, K.A., Kumar, V.H., Ryan, R.M., Swartz, D.D., Csiszar, K., Fong, K.S., 2007. Dysregulation of pulmonary elastin synthesis and assembly in preterm lambs with chronic lung disease. Am. J. Physiol. Lung Cell. Mol. Physiol. 292, L1370–L1384.

Chuang, P.T., Kawcak, T., McMahon, A.P., 2003. Feedback control of mammalian Hedgehog signaling by the Hedgehog-binding protein, Hip1, modulates Fgf signaling during branching morphogenesis of the lung. Genes Dev. 17, 342–347.

Coalson, J.J., 2003. Pathology of new bronchopulmonary dysplasia. Semin. Neonatol. 8, 73–81.

Coraux, C., Delplanque, A., Hinnrasky, J., Peault, B., Puchelle, E., Gaillard, D., 1998. Distribution of integrins during human fetal lung development. J. Histochem. Cytochem. 46, 803–810.

De Arcangelis, A., Mark, M., Kreidberg, J., Sorokin, L., Georges-Labouesse, E., 1999. Synergistic activities of alpha3 and alpha6 integrins are required during apical ectodermal ridge formation and organogenesis in the mouse. Development 126, 3957–3968.

De Langhe, S.P., Sala, F.G., Del Moral, P.M., Fairbanks, T.J., Yamada, K.M., Warburton, D., Burns, R.C., Bellusci, S., 2005. Dickkopf-1 (DKK1) reveals that fibronectin is a major target of Wnt signaling in branching morphogenesis of the mouse embryonic lung. Dev. Biol. 277, 316–331.

Dieperink, H.I., Blackwell, T.S., Prince, L.S., 2006. Hyperoxia and apoptosis in developing mouse lung mesenchyme. Pediatr. Res. 59, 185–190.

Fanaroff, A.A., Stoll, B.J., Wright, L.L., Carlo, W.A., Ehrenkranz, R.A., Stark, A.R., Bauer, C.R., Donovan, E.F., Korones, S.B., Laptook, A.R., Lemons, J.A., Oh, W., Papile, L.A., Shankaran, S., Stevenson, D.K., Tyson, J.E., Poole, W.K., 2007. Trends in neonatal morbidity and mortality for very low birthweight infants. Am. J. Obstet. Gynecol. 196 (147), e1–8.

Haas, C.S., Amann, K., Schittny, J., Blaser, B., Muller, U., Hartner, A., 2003. Glomerular and renal vascular structural changes in alpha8 integrin-deficient mice. J. Am. Soc. Nephrol. 14, 2288–2296.

Hartner, A., Cordasic, N., Klanke, B., Muller, U., Sterzel, R.B., Hilgers, K.F., 2002. The alpha8 integrin chain affords mechanical stability to the glomerular capillary tuft in hypertensive glomerular disease. Am. J. Pathol. 160, 861–867.

Kramer, B.W., Kallapur, S., Newnham, J., Jobe, A.H., 2008. Prenatal inflammation and lung development. Semin. Fetal. Neonatal. Med.

Kreidberg, J.A., Donovan, M.J., Goldstein, S.L., Rennke, H., Shepherd, K., Jones, R.C., Jaenisch, R., 1996. Alpha 3 beta 1 integrin has a crucial role in kidney and lung organogenesis. Development 122, 3537–3547.

Le Cras, T.D., Hardie, W.D., Deutsch, G.H., Albertine, K.H., Ikegami, M., Whitsett, J.A., Korfhagen, T.R., 2004. Transient induction of TGF-alpha disrupts lung morphogenesis, causing pulmonary disease in adulthood. Am. J. Physiol. Lung Cell. Mol. Physiol. 287, L718–L729.

Lim, L., Kalinichenko, V.V., Whitsett, J.A., Costa, R.H., 2002. Fusion of lung lobes and vessels in mouse embryos heterozygous for the forkhead box f1 targeted allele. Am. J. Physiol. Lung Cell. Mol. Physiol. 282, L1012–L1022.

Linton, J.M., Martin, G.R., Reichardt, L.F., 2007. The ECM protein nephronectin promotes kidney development via integrin alpha8beta1-mediated stimulation of Gdnf expression. Development 134, 2501–2509.

Maeda, Y., Dave, V., Whitsett, J.A., 2007. Transcriptional control of lung morphogenesis. Physiol. Rev. 87, 219–244.

Metzger, R.J., Klein, O.D., Martin, G.R., Krasnow, M.A., 2008. The branching programme of mouse lung development. Nature 453, 745–750.

Moss, T.J., Newnham, J.P., Willett, K.E., Kramer, B.W., Jobe, A.H., Ikegami, M., 2002. Early gestational intra-amniotic endotoxin: lung function, surfactant, and morphometry. Am. J. Respir. Crit. Care Med. 165, 805–811.

Motoyama, J., Liu, J., Mo, R., Ding, Q., Post, M., Hui, C.C., 1998. Essential function of Gli2 and Gli3 in the formation of lung, trachea and oesophagus. Nat. Genet. 20, 54–57.

Muller, U., Wang, D., Denda, S., Meneses, J.J., Pedersen, R.A., Reichardt, L.F., 1997. Integrin alpha8beta1 is critically important for epithelial-mesenchymal interactions during kidney morphogenesis. Cell 88, 603–613.

Nakamura, Y., Funatsu, Y., Yamamoto, I., Yamana, K., Nishimura, T., Hosokawa, Y., Fukuda, S., Nakashima, H., Tsunosue, M., Hashimoto, T., et al., 1985. Potter's syndrome associated with renal agenesis or dysplasia. Morphological and biochemical study of the lung. Arch. Pathol. Lab. Med. 109, 441–444.

Nguyen, N.M., Miner, J.H., Pierce, R.A., Senior, R.M., 2002. Laminin alpha 5 is required for lobar septation and visceral pleural basement membrane formation in the developing mouse lung. Dev. Biol. 246, 231–244.
Perlman, M., Williams, J., Hirsch, M., 1976. Neonatal pulmonary hypoplasia after prolonged leakage of amniotic fluid. Arch. Dis. Child. 51, 349–353.
Prince, L.S., Dieperink, H.I., Okoh, V.O., Fierro-Perez, G.A., Lallone, R.L., 2005. Toll-like receptor signaling inhibits structural development of the distal fetal mouse lung. Dev. Dyn. 233, 553–561.
Prince, L.S., Okoh, V.O., Moninger, T.O., Matalon, S., 2004. Lipopolysaccharide increases alveolar type II cell number in fetal mouse lungs through Toll-like receptor 4 and NF-kappaB. Am. J. Physiol. Lung. Cell. Mol. Physiol. 287, L999–1006.
Roman, J., 1997. Fibronectin and fibronectin receptors in lung development. Exp. Lung Res. 23, 147–159.
Roth-Kleiner, M., Post, M., 2005. Similarities and dissimilarities of branching and septation during lung development. Pediatr. Pulmonol. 40, 113–134.
Sakai, T., Larsen, M., Yamada, K.M., 2003. Fibronectin requirement in branching morphogenesis. Nature 423, 876–881.
Schnapp, L.M., Breuss, J.M., Ramos, D.M., Sheppard, D., Pytela, R., 1995a. Sequence and tissue distribution of the human integrin alpha 8 subunit: a beta 1-associated alpha subunit expressed in smooth muscle cells. J. Cell. Sci. 108 (Pt. 2), 537–544.
Schnapp, L.M., Hatch, N., Ramos, D.M., Klimanskaya, I.V., Sheppard, D., Pytela, R., 1995b. The human integrin alpha 8 beta 1 functions as a receptor for tenascin, fibronectin, and vitronectin. J. Biol. Chem. 270, 23196–23202.
Sinkin, R.A., Roberts, M., LoMonaco, M.B., Sanders, R.J., Metlay, L.A., 1998. Fibronectin expression in bronchopulmonary dysplasia. Pediatr. Dev. Pathol. 1, 494–502.
Speer, C.P., 2003. Inflammation and bronchopulmonary dysplasia. Semin. Neonatol. 8, 29–38.
Thibeault, D.W., Mabry, S.M., Ekekezie, II, Zhang, X., Truog, W.E., 2003. Collagen scaffolding during development and its deformation with chronic lung disease. Pediatrics 111, 766–776.
Wang, A., Patrone, L., McDonald, J.A., Sheppard, D., 1995. Expression of the integrin subunit alpha 9 in the murine embryo. Dev. Dyn. 204, 421–431.
Warburton, D., Schwarz, M., Tefft, D., Flores-Delgado, G., Anderson, K.D., Cardoso, W.V., 2000. The molecular basis of lung morphogenesis. Mech. Dev. 92, 55–81.
Weibel, E.R., Kistler, G.S., Scherle, W.F., 1966. Practical stereological methods for morphometric cytology. J. Cell. Biol. 30, 23–38.
Willet, K.E., Jobe, A.H., Ikegami, M., Kovar, J., Sly, P.D., 2001. Lung morphometry after repetitive antenatal glucocorticoid treatment in preterm sheep. Am. J. Respir. Crit. Care Med. 163, 1437–1443.
Wu, J.E., Santoro, S.A., 1996. Differential expression of integrin alpha subunits supports distinct roles during lung branching morphogenesis. Dev. Dyn. 206, 169–181.
Young, K.C., Del Moral, T., Claure, N., Vanbuskirk, S., Bancalari, E., 2005. The association between early tracheal colonization and bronchopulmonary dysplasia. J. Perinatol. 25, 403–407.
Young, S.L., Chang, L.Y., Erickson, H.P., 1994. Tenascin-C in rat lung: distribution, ontogeny and role in branching morphogenesis. Dev. Biol. 161, 615–625.